The Self-Calibration Method for the Vertex Distance of the Elliptical Paraboloid Array

Zekui Lv [1,†] , Zhikun Su [1,†] , Dong Zhang [1], Lingyu Gao [1], Zhiming Yang [1], Fengzhou Fang [2,*] , Haitao Zhang [3,*] and Xinghua Li [1,*]

1 State Key Laboratory of Precision Measuring Technology and Instruments, School of Precision Instruments and Opto-electronics Engineering, Tianjin University, Tianjin 300072, China
2 Centre of Micro/Nano Manufacturing Technology, University College Dublin, D04 V1W8 Dublin, Ireland
3 Key Laboratory of Advanced Transducers and Intelligent Control System, Ministry of Education, Taiyuan University of Technology, Taiyuan 030024, China
* Correspondence: Fengzhou.Fang@ucd.ie (F.F.); zhanghaitao@tyut.edu.cn (H.Z.); lixinghua@tju.edu.cn (X.L.)
† These authors contributed equally to this work.

check for updates

Abstract: The elliptical paraboloid array plays an important role in precision measurement, astronomical telescopes, and communication systems. The calibration of the vertex distance of elliptical paraboloids is of great significance to precise 2D displacement measurement. However, there are some difficulties in determining the vertex position with contact measurement. In this study, an elliptical paraboloid array and an optical slope sensor for displacement measurement were designed and analyzed. Meanwhile, considering the geometrical relationship and relative angle between elliptical paraboloids, a non-contact self-calibration method for the vertex distance of the elliptical paraboloid array was proposed. The proposed self-calibration method was verified by a series of experiments with a high repeatability, within 3 μm in the X direction and within 1 μm in the Y direction. Through calibration, the displacement measurement system error was reduced from 100 μm to 3 μm. The self-calibration method of the elliptical paraboloid array has great potential in the displacement measurement field, with a simple principle and high precision.

Keywords: elliptical paraboloid array; self-calibration method; vertex distance; optical slope sensor; geometric relationship; relative angle

1. Introduction

Sensor arrays are widely used in modern scientific research and industrial production [1–3]. Depending on the application requirements, sensor arrays can be designed with different geometries, including those that are linear [4], circular [5], planar [6], L-shaped [7], and so on. Rui et al. [8] proposed a capacitance-sensor-array-based imaging system to detect water leakage inside insulating slabs with porous cells. Tan et al. [9] developed a giant magneto resistance sensor array which included various types of small gaps, curling wires, wide fractures, and abrasion to detect defects in various types of wire rope. Gao et al. [10] utilized a large area sinusoidal grid surface array as the measurement reference of a surface encoder for multi-axis position measurement. Wu et al. [11] presented a novel instrumentation system, including an infrared laser source and a photodiode sensor array, to provide an accurate measurement of the gas void fraction of two-phase CO_2 flow. Dario [12] demonstrated a novel sensor array based on SnO_2, CuO, and WO_2 nanowires, which is able to discriminate four typical compounds added to food products. Atte et al. [13] demonstrated that the bioimpedance sensor array has the ability to achieve long-term monitoring of intact skin and acute wound healing from beneath primary dressings. Forough et al. [14] developed a fluorometric sensor array for the detection of TNT

(trinitrotoluene), DNT (dinitrotoluene), and TNP (trinitrophenyl), which demonstrated a promising capacity to detect structurally similar nitroaromatics in mixtures and the complex media of soil and groundwater samples. The advantage of using a sensor array instead of a single sensor is that the array adds new dimensions to the observations, helping to estimate more parameters and improve the estimation performance. Of course, the calibration of relevant parameters is a requirement that cannot be ignored before using the sensor array.

Zhang et al. [15] described a method for calibrating the distances between the balls of a 1-D ball array using a specially designed device with a laser interferometer, which gives the distances between the balls in two directions. Ouyang et al. [16] proposed a new alternative method for calibrating the ball array based on a CMM (coordinate measuring machine) and a gage block. To obtain a high accuracy in ball calibration, repeated measurements of the balls must be taken at least 10 times. Guenther et al. [17] introduced a self-calibration method for a ball plate, through which not only the pitch position of the balls, but also their radial and height position on the circular ball plate, were calibrated. Through computing the intersections of 2π-phase lines to detect the phase-shifting wedge grating arrays centers, Tao et al. [18] completed camera calibration. Xu et al. [19] presented a calibration method for a camera array and a rectification method for generating a light field image from the captured images. Zhang et al. [20] used a high-precision machine developed by the research of Halcon to measure the aperture diameter and aperture distance of a microstructure array. Solórzano et al. [21] presented a calibration model that can be extended to uncalibrated replicas of sensor arrays without acquiring new samples, favoring mass-production applications for gas sensor arrays. Sun et al. [22] purposed a new array geometry calibration method for underwater compact arrays to improve the robustness and accuracy of the calibration results. Zhai et al. [23] researched a calibration method for an array complementary metal–oxide–semiconductor photodetector using a black-box calibration device and an electrical analog delay method to address the disadvantages of traditional PMD (photonic mixer device) solid-state array lidar calibration methods. Through the above research, it can be concluded that the calibration of sensor arrays is helpful to improve their accuracy and practicability.

Elliptical paraboloid arrays have considerable application potential in the accurate detection of machine geometry errors. Nowadays, the elliptical paraboloid used in the field of precision measurement has a small surface area and high machining accuracy. To expand the measuring range of displacement, the elliptical paraboloid array has become a research focus. However, the calibration method for the vertex distance of the elliptical paraboloid array has seldom been investigated. There are two reasons accounting for this. On the one hand, contact measurement will destroy the surface properties of the elliptical paraboloid, and they are too small to be detected by probe. On the other hand, traditional visual inspection methods are often affected by specular images and ignore the relative angle between the elliptical paraboloids.
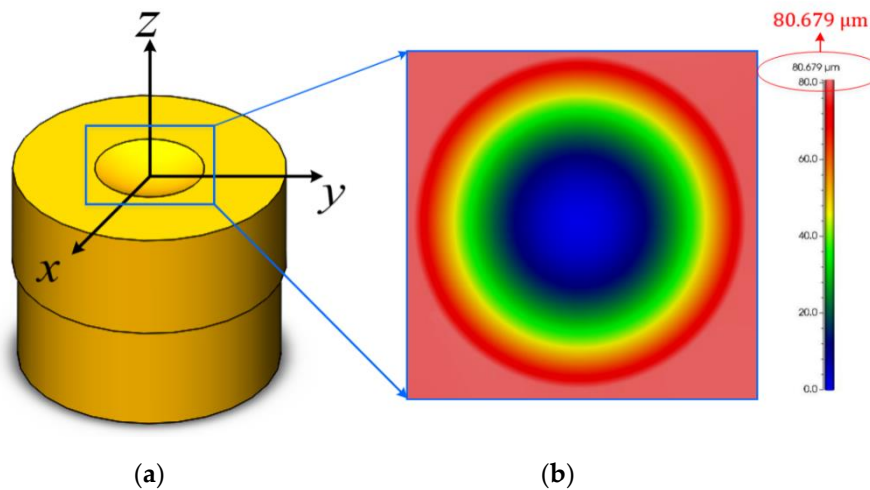
To overcome the above difficulties, a self-calibration method for the vertex distance of the elliptical paraboloid array using a non-contact optical slope sensor is proposed. A self-calibration method utilizes the existing displacement measurement system to achieve calibration with a low cost and convenient operation. The relative angle and geometric relationship between elliptical paraboloids was considered in the self-calibration method to improve the calibration accuracy. This self-calibration method has the characteristics of a high accuracy and high repeatability, is non-destructive, and has a long adaptive distance. After calibration, the displacement measurement system error was reduced from 100 μm to 3 μm, which satisfies the measuring requirement.

2. Materials and Methods
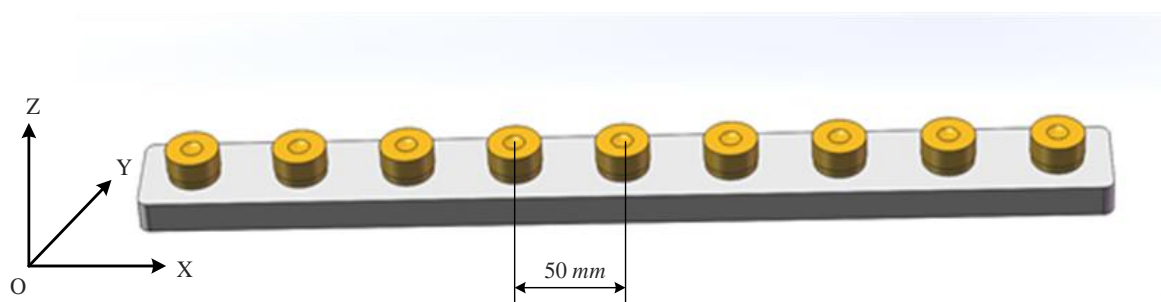
2.1. Elliptical Paraboloid Array

The elliptical paraboloid is a common type of quadric surface, which has wide application prospects in the field of precision measurement. As shown in Figure 1a, the three-dimensional model of the elliptical paraboloid with a superior optical reflection performance was machined by an

ultra-precision single-point diamond lathe. The processing quality of the elliptical paraboloid was detected by an optical 3D surface profiler, and the results are shown in Figure 1b. In Figure 1b, different colors in the image represent different depths. According to Figure 1b, it can be seen that the machining height (80.679 μm) and contour of the elliptical paraboloid are consistent with the theoretical design.

(**a**)   (**b**)

Figure 1. The model of the elliptical paraboloid and detection results of the 3D surface profile: (**a**) the model of the elliptical paraboloid; (**b**) the 3D surface profile for the model.

Lv et al. have described in detail the principle of 2D micro-displacement based on a single elliptical paraboloid [24]. However, the range of this measurement system is limited by the surface area of the elliptical paraboloid. A larger elliptical paraboloid will cause inconvenience in manufacturing and application. In this paper, a linear elliptical paraboloid array is proposed, in which the distance of the centers between adjacent elliptical paraboloids is only 50 mm in the X direction. As shown in Figure 2, due to the existence of machining errors and installation errors, the vertex distance of the actual elliptical paraboloid array may be biased in both the X and Y directions. Therefore, it is our responsibility to accurately calibrate the vertex distance between elliptical paraboloids in the array to reduce systematic errors in actual applications.

Figure 2. The linear elliptical paraboloid array.

2.2. Optical Slope Sensor

The optical slope sensor used for the self-calibration method consists of a laser, a reflector, a spatial filter, a beam splitter, two lenses, a CCD (charge coupled device) camera, and more, as shown in Figure 3. The laser emitted from a laser source (power 5 mW, wavelength λ = 650 nm, unpolarized light) is reflected by a reflector (offset 135°angle in a horizontal direction) and passes through a spatial filter (diameter 300 μm). After going through the spatial filter and focusing Lens 1 (focal length 30 mm), the laser beam is divided into two beams by the beam splitter (reflection factor of 50%). The reflected

beam, as the measuring beam, reaches the surface of the elliptical paraboloid array and is reflected again. Finally, the measuring beam is received by a CCD camera (pixels number 2592 × 1944, pixel size 2.2 × 2.2 μm) located on the focal plane of object Lens 2 (focal length 100 mm) and is transmitted to the computer for analysis and processing. The actual spot image is displayed on the computer screen in Figure 3, whose central position will be determined by the centroid algorithm. Through the processing of the spot image, the angle and displacement can be calculated precisely. In short, the optical slope sensor is simple, portable, and accurate.
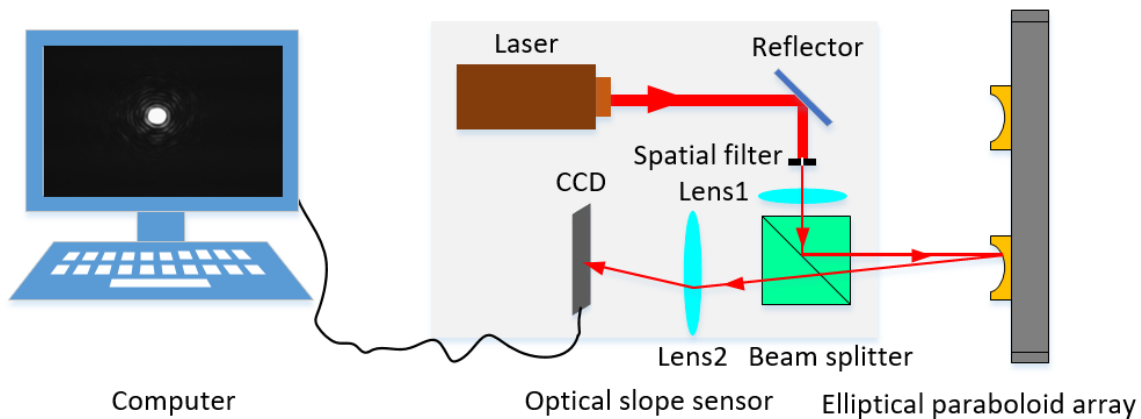

Figure 3. Schematic diagram of the optical slope sensor.

2.3. Experimental Apparatus

Experiments to certify the self-calibration method for the vertex distance of the elliptical paraboloid array were undertaken several times with the help of an XL80 laser interferometer with a resolution of 0.001 μm and system accuracy of ±0.5 ppm (Renishaw, Gloucestershire, UK), and a Brown & Sharpe Chameleon 9159 bridge-type coordinate measuring machine (CMM) with a technical target of U12.3 + 2.8 L/1000 (Hexagon, Stockholm, Sweden). The experimental apparatus of the self-calibration system is shown in Figure 4. The optical slope sensor mounted on the quill of the CMM moves along the direction of the elliptical paraboloid array, whose direction is parallel to the X direction of the CMM. The function of the laser interferometer is to monitor the actual displacement of the quill for accurate calibration. It should be noted that the apparatus of the calibration experiment is also suitable for the measurement experiment, which is the reason the method is called self-calibration.
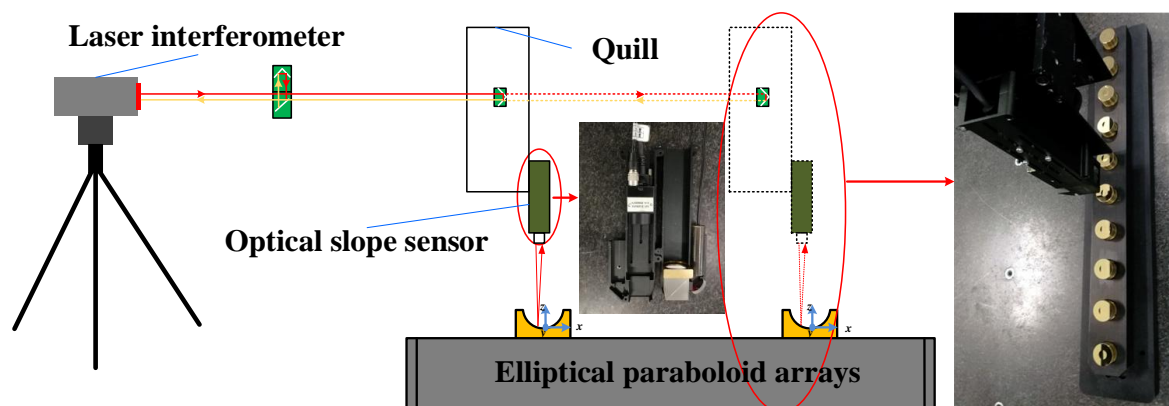

Figure 4. Experimental apparatus of the calibration system.

2.4. Mathematical Model

As shown in Figure 5, the vertex distance between elliptical paraboloid i and j is d_x and d_y in the X and Y direction, respectively. First, point A on the elliptical paraboloid i is measured by the optical slope sensor to obtain the light spot central position (x_{cA}, y_{cA}). Then, an optical slope sensor moves about 50 mm along the X direction to point B on the elliptical paraboloid j and the central position (x_{cB}, y_{cB}) is acquired. Point A' is the mapping point of point A, which means that point A' and point A will be in the same position if they are on an identical elliptical paraboloid. Therefore, the distance between point A' and point A is the same as the vertex distance of two elliptical paraboloids.
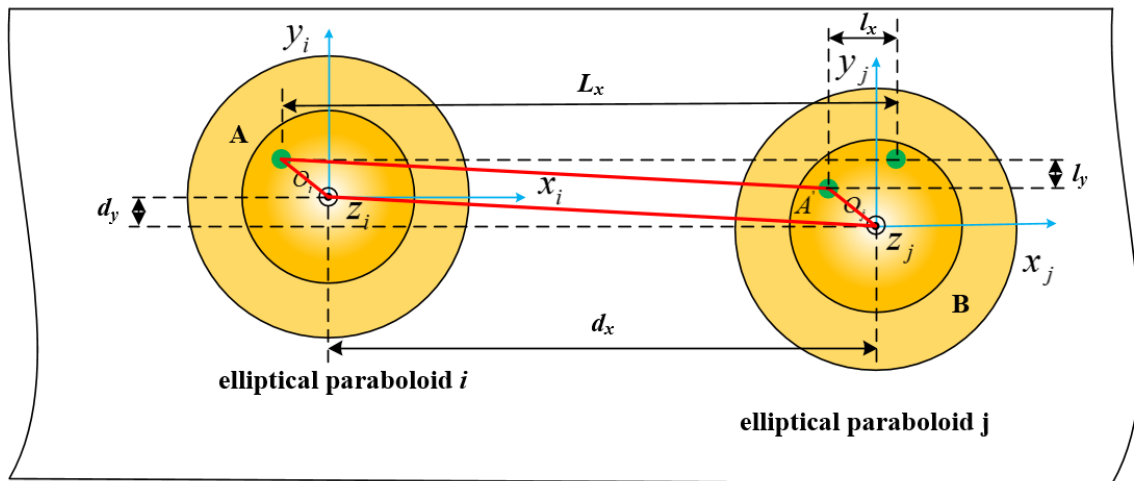

Figure 5. Calibration principle according to the geometric relationship.

According to the geometric relationship in Figure 5, the following equation can be determined:

$$\begin{cases} d_x = L_x - l_x \\ \quad d_y = l_y \end{cases} \tag{1}$$

where l_x and l_y are the distance between point A' and B, and L_x is the length between point A and B along the X direction monitored by a laser interferometer. l_x and l_y are calculated by displacement of the spot, as follows:

$$\begin{cases} l_x = (x_{cB} - x_{cA})c_1 \\ l_y = (y_{cB} - y_{cA})c_1 \end{cases} \tag{2}$$

where c_1 represents the displacement coefficient that needs to be calibrated.

The above model used the calibration formula in the case of only translation occurring between the elliptical paraboloids. However, the relative angular (pitch and yaw) elliptical Y and X axis between them is neglected. The pitch between two elliptical paraboloids is shown in Figure 6, which will result in the influence on spot displacement. The relative pitch ($\Delta\theta$) and yaw ($\Delta\varphi$) between each elliptical paraboloid should be calibrated, and their influence on displacement can be calculated by the following formula:

$$\begin{cases} x_{cA'} - x_{cA} = \Delta\theta / c_2 \\ y_{cA'} - y_{cA} = \Delta\varphi / c_2 \end{cases} \tag{3}$$

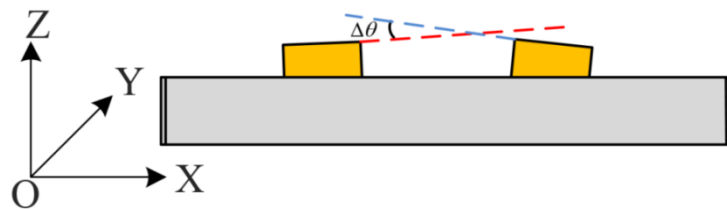where c_2 represents the angle coefficient that needs to be calibrated.

Figure 6. The pitch between two elliptical paraboloids.

Finally, the calibration formula for the vertex distance between paraboloids can be expressed as

$$\begin{cases} d_x = L_x - (x_{cB} - x_{cA} - \Delta\theta/c_2)c_1 \\ d_y = (y_{cB} - y_{cA} - \Delta\varphi/c_2)c_1 \end{cases} \tag{4}$$

2.5. Calibration Procedure

The procedure of calibration for the elliptical paraboloid array is shown in Figure 7.
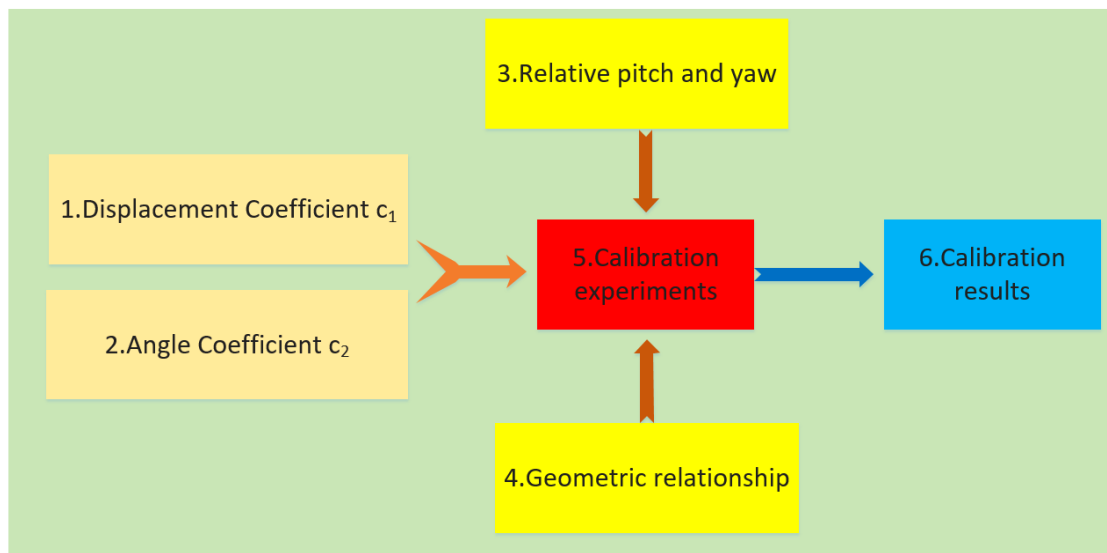

Figure 7. Calibration procedure.

Step one: The displacement coefficient c_1 is calibrated. The displacement coefficient c_1 refers to the actual displacement (μm) change corresponding to a change of a 1 μm length of the spot on the CCD camera. The calibration results for the displacement coefficient are shown in Figure 8. We verified that the displacement coefficient is about 3.5045 from the linear fitting equation, with a correlation coefficient of 0.9999.
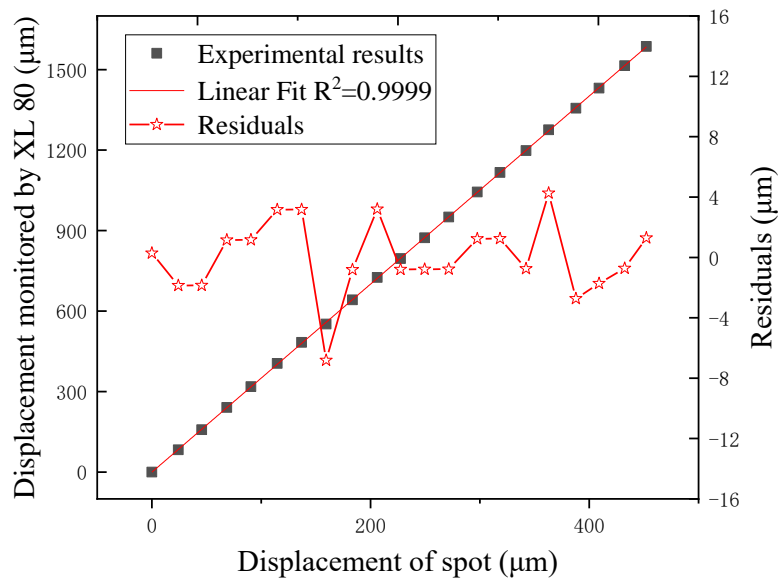
Figure 8. Calibration results in the X direction.

Step two: The angle coefficient c_2 is calibrated. The angle coefficient c_2 is described as the angular (arcsec) change associated with the 1 μm spot position on the CCD camera. The experimental results for angle coefficient calibration are shown in Figure 9. Figure 9 indicates that the result of the angle coefficient is approximately 4.975 from the linear fitting equation, with a correlation coefficient of 0.9999.
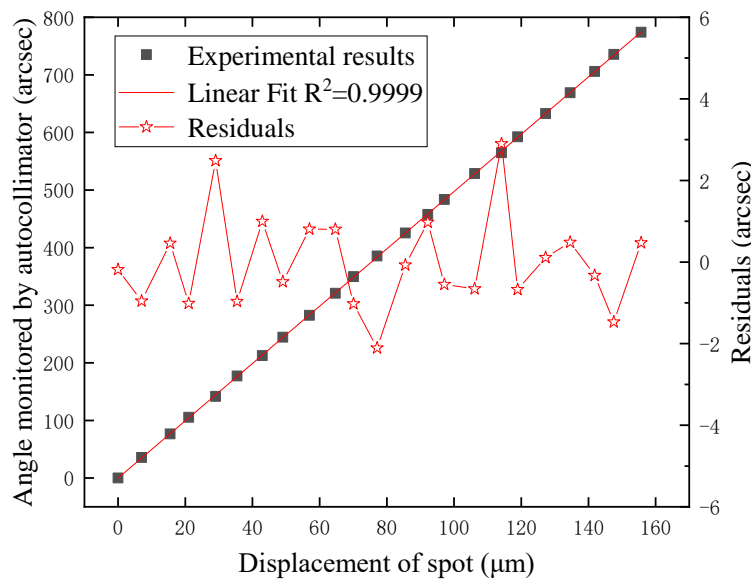

Figure 9. Calibration results in the Y direction.

Step three: Calculate the relative angles between elliptical paraboloids, including the pitch angle and yaw angle, using the optical slope sensor.

Step four: Consider the geometric relationship between the vertices and measuring points of the elliptical paraboloids, which is the basic principle of the whole calibration method.

Step five: Conduct calibration experiments. The quill of CMM moves 50 mm each time to reach the position of the next elliptical paraboloid; meanwhile, the light spot central position is recorded.

Step six: Analyze and compare calibration results. The calibration results require analysis and comparison to prove their correctness, especially in practical applications.

3. Experimental Results

3.1. Relative Pitch and Yaw

Before the experiment, it was obvious that the ring surrounding the elliptical paraboloid was machined into a mirror plane whose *pv* (peak to valley) was 0.038 μm. The reflection characteristics of the rings were similar to a K9 standard precision planar mirror. Therefore, the optical angle sensor based on the self-collimation principle and the ring could be utilized to measure the two-dimensional angle (pitch and yaw). Ultra-precision machining requires a guarantee that the optical axis of the elliptical paraboloid and the normal vector of the ring have good parallelism. Therefore, detection of the pitch and yaw of each elliptical paraboloid is replaced by each ring. The elliptical paraboloid array was placed along the X direction of the CMM, and the optical slope sensor was mounted on the quill of the CMM to perform multi-point measurement on each of the rings. Taking the first elliptical paraboloid as an angle reference, the relative pitch angle and yaw angle of other elliptical paraboloids could be obtained. The average result is shown in Table 1. According to Table 1, the relative pitch angle and yaw angle are clearly calibrated within 200″, which is due to installation and adjustment of the elliptical paraboloid.

Table 1. Calibration results of the relative pitch angle and yaw angle.

Elliptical Paraboloid	Relative Pitch Angle/Arcsec	Relative Yaw Angle/Arcsec
1	0	0
2	−149.8	103.9
3	−81.7	124.3
4	176.7	−71.5
5	186.5	155.8
6	82.7	−34.0
7	107.1	−92.2
8	−44.1	166.7
9	−175.4	185.7

3.2. Calibration Results

The calibration experiment was carried out three times, and the experimental results are shown in Figure 10. In order to eliminate the influence of errors caused by a single measurement, the average of three measurements was taken as the final calibration result, which is shown in Table 2. As can be seen from Figure 10, the calibration results have a good repeatability in both the X and Y directions. Through three repetitive experiments, we can conclude that the difference between them was within 3 μm in the X direction and within 1 μm in the Y direction. The experimental results shown in Table 2 are approaching the theoretical design values in two directions, which directly proves the correctness of the calibration method.

Table 2. Calibration results of the elliptical paraboloid array.

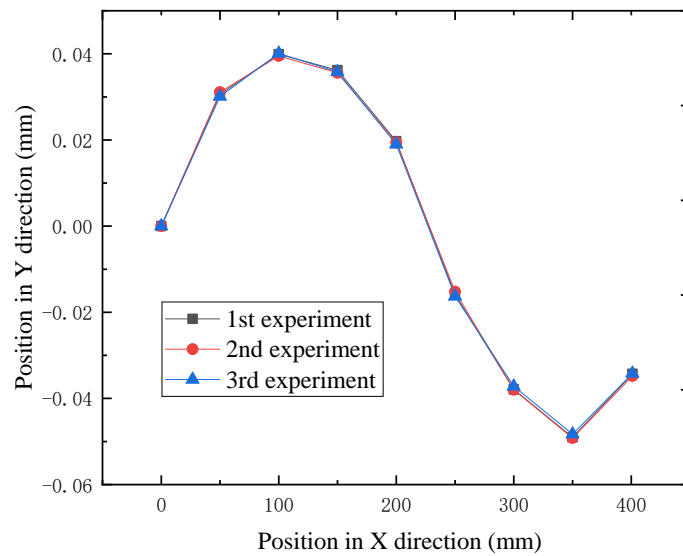| Type	1	2	3	4	5	6	7	8	9
X/mm	0	49.9681	100.0044	149.9427	199.9558	250.0217	300.0113	350.0063	400.0362
Y/mm	0	0.0306	0.0398	0.0359	0.0194	−0.0158	−0.0377	0.0488	−0.0344

Figure 10. Repeatability of the calibration experiment.

3.3. Comparison Experiment

In order to verify the effect of system calibration, a comparison experiment were carried out in the same laboratory environment. The direction of the elliptical paraboloid array was adjusted to be parallel to the Y direction of the CMM. Correspondingly, the optical slope sensor was mounted on the quill to move in the Y direction. The measured data were processed with the calibration results and the original design values as reference values in turn. The comparison results in the moving direction are shown in Figure 11. As shown in Figure 11, the error of the measurement results before calibration is less than 100 μm due to the influence of installation and manufacture. However, the experimental results after system calibration show that the measurement error is controlled within 3 μm in the moving direction, which satisfies the requirement of the displacement measurement accuracy. Therefore, we can say that the necessity and correctness of system calibration have been proven by the comparison experiment. In fact, the calibration experiment results compensate for the displacement measurement error of the system in a sense.
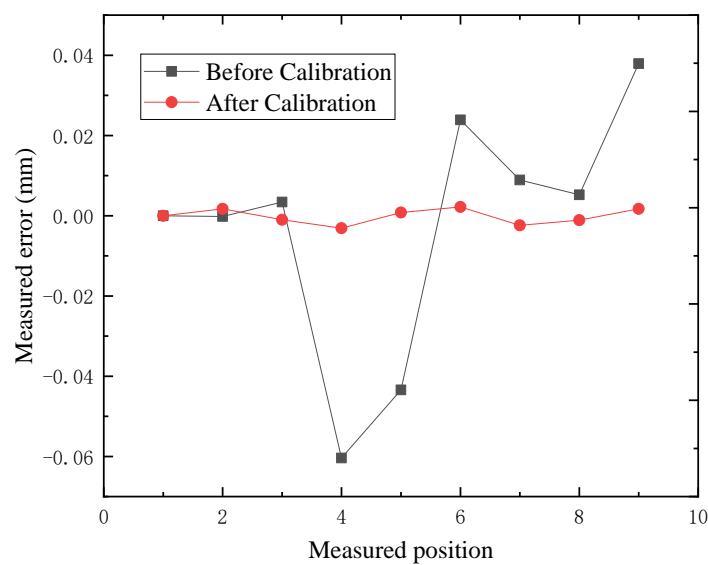

Figure 11. Comparison experiment.

4. Conclusions

The present study was designed to research a self-calibration method with respect to the vertex distance of the elliptical paraboloid array, which solves the benchmark problem in long-range displacement measurements. The self-calibration method, which was based on the geometric relationships between elliptical paraboloids, was verified by experiments using a Renishaw XL80, Hexagon CMM, and optical slope sensor designed by ourselves. The results of these experiments show that the calibration results are consistent with the design values, and the repeatability was within 3 μm in the X direction and within 1 μm in the Y direction. In addition, the comparison experiment proved that the displacement measurement system error was reduced from 100 μm to 3 μm after calibration. The results show that the self-calibration method can meet the calibration requirements of the elliptical paraboloid array, which lays a solid foundation for subsequent experiments related to displacement measurement. In order to improve the accuracy of the calibration results, it would be necessary to select high-precision motion guides and ensure that their motion direction is parallel to the elliptical paraboloid array. Further studies need to be carried out in order to validate the application value of the elliptical paraboloid array in the displacement-related measurement field, such as by focusing on the positioning error, straightness error, and perpendicularity error.

Author Contributions: X.L., F.F., and H.Z. proposed the method and modified the paper; Z.L. designed the experiments and wrote the paper; D.Z. and L.G. developed the system software and processed the data; Z.S. and Z.Y. designed the mechanical and optical structure.

Conflicts of Interest: The authors declare no conflicts of interest.

References

1. GhazaI, N.; Ebrahim, G.-Z.; Antoine, L.; Mohamad, S. Smart Cell Culture Monitoring and Drug Test Platform Using CCD Capacitive Sensor Array. *IEEE Trans. Biomed. Eng.* **2019**, *66*, 1094–1104.
2. Jie, H.; Hanmin, P.; Ting, M.; Tingyu, L.; Mingsen, G.; Penghui, L.; Yalei, B.; Chunsheng, Z. An airflow sensor array based on polyvinylidene fluoride cantilevers for synchronously measuring airflow direction and velocity. *Flow Meas. Instrum.* **2019**, *67*, 166–175.
3. Kaisti, M.; Panula, T.; Leppänen, J.; Punkkinen, R.; Tadi, M.J.; Vasankari, T.; Meriheinä, U. Clinical assessment of a non-invasive wearable MEMS pressure sensor array for monitoring of arterial pulse waveform, heart rate and detection of atrial fibrillation. *NPJ Digit. Med.* **2019**, *39*, 1–10. [CrossRef] [PubMed]
4. Zhong, Y.; Xiang, J.; Chen, X.; Jiang, Y.; Pang, J. Multiple Signal Classification-Based Impact Localization in Composite Structures Using Optimized Ensemble Empirical Mode Decomposition. *Appl. Sci.* **2018**, *8*, 1447. [CrossRef]
5. Cui, X.; Yan, Y.; Guo, M.; Han, X.; Hu, Y. Localization of CO_2 Leakage from a Circular Hole on a Flat-Surface Structure Using a Circular Acoustic Emission Sensor Array. *Sensors* **2016**, *16*, 1951. [CrossRef] [PubMed]
6. Chung, S.; Park, T.; Park, S.; Kim, J.; Park, S.; Son, D.; Cho, S. Colorimetric Sensor Array for White Wine Tasting. *Sensors* **2015**, *15*, 18197–18208. [CrossRef]
7. Si, W.; Zhao, P.; Qu, Z. Two-Dimensional DOA and Polarization Estimation for a Mixture of Uncorrelated and Coherent Sources with Sparsely-Distributed Vector Sensor Array. *Sensors* **2016**, *16*, 789. [CrossRef]
8. Li, R.; Li, Y.; Peng, L. An Electrical Capacitance Array for Imaging of Water Leakage inside Insulating Slabs with Porous Cells. *Sensors* **2019**, *19*, 2514. [CrossRef]
9. Tan, X.; Zhang, J. Evaluation of Composite Wire Ropes Using Unsaturated Magnetic Excitation and Reconstruction Image with Super-Resolution. *Appl. Sci.* **2018**, *8*, 767. [CrossRef]
10. Gao, W.; Araki, T.; Kiyono, S.; Okazaki, Y.; Yamanaka, M. Precision nano-fabrication and evaluation of a large area sinusoidal grid surface for a surface encoder. *Precis. Eng.* **2003**, *27*, 289–298. [CrossRef]
11. Wu, H.; Duan, Q. Gas Void Fraction Measurement of Gas-Liquid Two-Phase CO_2 Flow Using Laser Attenuation Technique. *Sensors* **2019**, *19*, 3178. [CrossRef] [PubMed]

12. Zappa, D. Low-Power Detection of Food Preservatives by a Novel Nanowire-Based Sensor Array. *Foods* **2019**, *8*, 226. [CrossRef] [PubMed]

13. Kekonen, A.; Bergelin, M.; Johansson, M.; Kumar Joon, N.; Bobacka, J.; Viik, J. Bioimpedance Sensor Array for Long-Term Monitoring of Wound Healing from Beneath the Primary Dressings and Controlled Formation of H_2O_2 Using Low-Intensity Direct Current. *Sensors* **2019**, *19*, 2505. [CrossRef] [PubMed]

14. Ghasemi, F.; Hormozi-Nezhad, M.R. Determination and identification of nitroaromatic explosives by a double-emitter sensor array. *Talanta* **2019**, *201*, 230–236. [CrossRef] [PubMed]

15. Zhang, G.X.; Zang, Y.F. A method for machine geometry calibration using 1-D ball array. *CIRP Ann.* **1991**, *40*, 519–522. [CrossRef]

16. Ouyang, J.F.; Jawahir, I.S. Ball array calibration on a coordinate measuring machine using a gage block. *Measurement* **1995**, *16*, 219–229. [CrossRef]

17. Anke, G.; Dirk, S.; Gert, G. Self-Calibration Method for a Ball Plate Artefact on a CMM. *CIRP Ann.* **2016**, *65*, 503–506.

18. Tao, J.; Wang, Y.; Cai, B.; Wang, K. Camera Calibration with Phase-Shifting Wedge Grating Array. *Appl. Sci.* **2018**, *8*, 644. [CrossRef]

19. Xu, Y.; Maeno, K.; Nagahara, H.; Taniguchi, R.I. Camera array calibration for light field acquisition. *Front. Comput. Sci.* **2015**, *9*, 691–702. [CrossRef]

20. Zhang, X.; Liu, Q.; Yin, Z.; Zhao, R.; Lin, J. Research on In-situ Measurement System of Microstructure Array. *Modul. Mach. Tool Autom. Manuf. Tech.* **2018**, *6*, 93–97.

21. Solórzano, A.; Rodriguez-Perez, R.; Padilla, M.; Graunke, T.; Fernandez, L.; Marco, S.; Fonollosa, J. Multi-unit calibration rejects inherent device variability of chemical sensor arrays. *Sens. Actuators B Chem.* **2018**, *265*, 142–154. [CrossRef]

22. Sun, D.; Ding, J.; Zheng, C.; Huang, W. Array geometry calibration for underwater compact arrays. *Appl. Acoust.* **2019**, *145*, 374–384. [CrossRef]

23. Zhai, Y.; Song, P.; Chen, X. A Fast Calibration Method for Photonic Mixer Device Solid-State Array Lidars. *Sensors* **2019**, *19*, 822. [CrossRef] [PubMed]

24. Lv, Z.; Li, X.; Su, Z.; Zhang, D.; Yang, X.; Li, H.; Li, J.; Fang, F. A Novel 2D Micro-Displacement Measurement Method Based on the Elliptical Paraboloid. *Appl. Sci.* **2019**, *9*, 2517. [CrossRef]